Article type: Research Article

Tuning the Interfaces of ZnO/$ZnCr_2O_4$ Derived from Layered-Double-Hydroxide Precursors to Advance Nitrogen Photofixation

*Junyu Gao[a, b], Fan Wu[a, b], Yunxuan Zhao[a, c] *, Xuanang Bian[a, b], Chao Zhou[a], Junwang Tang[d] and Tierui Zhang[a, b,] **

((Optional Dedication))

J. Gao, F. Wu, Dr. Y. Zhao, X. Bian, Dr. C. Zhou, Prof. T. Zhang
[a]Key Laboratory of Photochemical Conversion and Optoelectronic Materials, Technical Institute of Physics and Chemistry, Chinese Academy of Sciences, Beijing, 100190, China
Fax: +86 10 62554670 Tel: +86 10 82543428
E-mail: yunxuan@mail.ipc.ac.cn; tierui@mail.ipc.ac.cn

J. Gao, F. Wu, X. Bian, Prof. T. Zhang
[b]Center of Materials Science and Optoelectronics Engineering, University of Chinese Academy of Sciences, Beijing, 100049, China

Dr. Y. Zhao
[c]College of Science, Hebei University of Science and Technology, Shijiazhuang, 050018, China

Prof. J. Tang
[d]Department of Chemical Engineering, University College London, WC1E 7JE London, United Kingdom

J. Gao and F. Wu contributed equally to this work.

Abstract: Drawing inspiration from the enzyme nitrogenase in nature, researchers are increasingly delving into semiconductor photocatalytic nitrogen fixation due to its similar surface catalytic processes. Herein, we reported a facile and efficient approach to achieving the regulation of $ZnO/ZnCr_2O_4$ photocatalysts with ZnCr-layered double hydroxide (ZnCr-LDH) as precursors. By optimizing the composition ratio of Zn/Cr in ZnCr-LDH to tune interfaces, we can achieve an enhanced nitrogen photofixation performance (an ammonia evolution rate of 31.7 $\mu mol\, g^{-1}\, h^{-1}$ using pure water as a proton source) under ambient conditions. Further, photo-electrochemical measurements and transient surface photovoltage spectroscopy revealed that the enhanced photocatalytic activity can be ascribed to the effective carrier separation efficiency, originating from the abundant composite interfaces. This work further demonstrated a promising and viable strategy for the synthesis of nanocomposite photocatalysts for nitrogen photofixation and other challenging photocatalytic reactions.

Introduction

As one of the most essential inorganic chemicals,[1] ammonia (NH_3) plays a crucial role in various fields, including agriculture, explosives, chemical synthesis and energy.[2-4] Consequently, the industry of synthetic ammonia occupies a pivotal position in the national economy.[5] Despite nitrogen being the most abundant gas in the Earth's atmosphere (around 78% by volume),[6] it is notoriously challenging to activate and dissociate molecular nitrogen for ammonia synthesis due to its formidable triple bond (942 kJ mol^{-1}).[7] In nature, the nitrogen fixation process occurs *via* the nitrogenase enzyme and atmospheric fixation by lightning strikes.[8] Industrially, Fritz Haber and Carl Bosch achieved a breakthrough in artificial ammonia synthesis using Fe-based catalysts in 1913.[9-10] However, this method accompanied by high energy consumption and carbon emission issues, has greatly hindered its sustainable future development.[11] Therefore, the search for an alternative pathway toward NH_3 synthesis using renewable energy has become a long-term goal. Harnessing clean solar energy as the driving force to enable nitrogen photofixation is an environmental-friendly and feasible synthetic route.[12-13] Further, the linchpin of this route lies in designing efficient photocatalysts capable of converting nitrogen directly to ammonia under ambient conditions.

Nowadays, whilst enormous advances regarding nitrogen photofixation have been made in previous studies,[14-16] the solar-to-ammonia conversion efficiency of photocatalyst is still too low to garner significant industrial interest.[17] The poor separation efficiency of photogenerated carriers is one of the intrinsic reasons. In response to this limitation, the utilization of heterojunction strategies has gained widespread recognition as an effective approach to enhancing the charge-transfer capability. Consequently, it is feasible to construct advantageous and impressive heterojunctions with tunable heterostructured interfaces, which can enable effective photocatalytic reduction of N_2 to NH_3.

Layered double hydroxides (LDHs), which can be represented by the general formula $[M^{2+}_{1-x}M^{3+}_{x}\ (OH)_2]^{q+}(A^{n-})_{q/n}\cdot yH_2O$ (where M^{2+} and M^{3+} refer to specific divalent and trivalent metal cations respectively, and A^{n-} are the charge balancing anions located between layers), exhibits a superior catalytic property in electrocatalysis and

photocatalysis due to their unique structure.[18] Meanwhile, LDHs can be served as precursors for the synthesis of new catalysts with affluent interfaces *via* calcination under different oxidizing or reducing atmospheres, such as heterojunctions and Schottky junctions.[19] In photocatalysis, the as-designed heterojunctions and Schottky junctions can effectively promote the separation of photogenerated carriers, thus boosting photocatalytic activity. Therefore, this synthetic strategy that using LDH as a precursor, will probably offer a practical means to tune heterostructured interfaces for high-efficiency nitrogen photofixation.

In this work, we fabricated a series of ZnO/$ZnCr_2O_4$ heterojunction photocatalysts derived from ZnCr-LDH precursor through a simple thermal process. By optimizing the composition ratio of Zn/Cr in ZnCr-LDH and calcination temperatures, we can directly regulate heterostructured interfaces in as-prepared ZnO/$ZnCr_2O_4$ and acquire a considerable NH_3 evolution rate of 31.5 μmol g^{-1} h^{-1}. Furthermore, a better nitrogen photocatalytic activity of ZnO/$ZnCr_2O_4$ heterojunction derived from LDH precursors can be acquired as compared with the ordinary ZnO/$ZnCr_2O_4$ samples prepared by other methods. The advanced performance can be attributed to the superior carrier separation efficiency, resulting from the unique interface structures in as-designed ZnO/$ZnCr_2O_4$ as verified by a number of photo-electrochemical measurements and transient surface photovoltage spectroscopy (TS-SPV).

Results and Discussion

Among various semiconductor photocatalysts, zinc-based materials have drew particular attention owing to their non-toxic and cost-effective nature. [20] Nonetheless, the low separation efficiency of photogenerated electrons and holes has hindered their practical application and further development in photocatalysis. To address this concern, semiconductor heterojunction has been extensively studied as a valuable method to improve the photogenerated carriers' separation efficiency (*e.g.*, ZnO and $ZnCr_2O_4$).[21-22] Theoretically, the bandgap and crystal structure of $ZnCr_2O_4$ are compatible with those of ZnO, making it an ideal candidate to form a novel heterostructure with ZnO.[23] In Figure 1a-b, the valence band maximum and conduction band minimum of ZnO gave the calculated bandgap of about 3.3 eV, and that of $ZnCr_2O_4$ is almost 3.4 eV, basically

consistent with the previous studies.[20-22] Moreover, the total and partial density of states were also presented in Figure 1c-d. Notably, the valence band (VB) of ZnO is mainly composed of Zn 3d and O 2p orbitals, while the conduction band (CB) is a contribution from the Zn 2s and O 2p orbitals. For $ZnCr_2O_4$, the hybridization orbitals of Cr 3d and O 2p are mainly occupying the VB, with the CB containing Cr 3d and O 2p orbitals. Combined with reported results and our calculated bandgaps,[23] the ZnO and $ZnCr_2O_4$ possessed the properties for forming an efficient heterojunction, and the photogenerated electrons in $ZnCr_2O_4$ would transfer to ZnO, corresponding to the transition of photogenerated holes to $ZnCr_2O_4$ (Figure S1). The enhanced separation efficiency of photogenerated carriers in as-designed ZnO/$ZnCr_2O_4$ is supported by the experimental results below, which enables it to achieve remarkable nitrogen photofixation capacity.

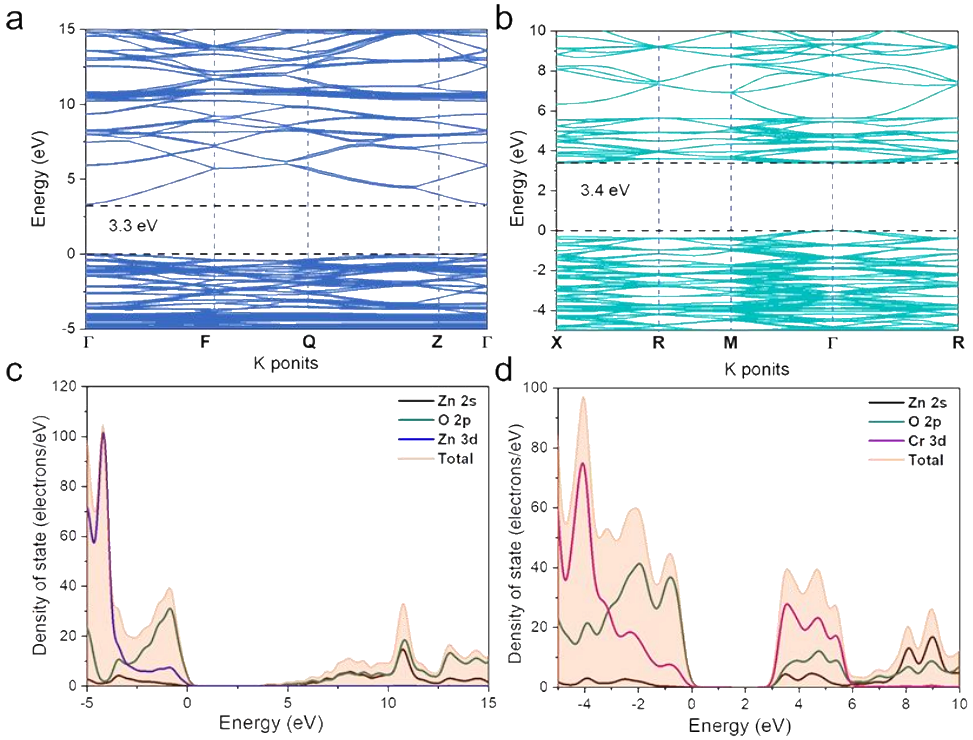

Figure 1. The calculated bandgap structures and corresponding density of states for (a, c) ZnO and (b, d) $ZnCr_2O_4$, respectively.

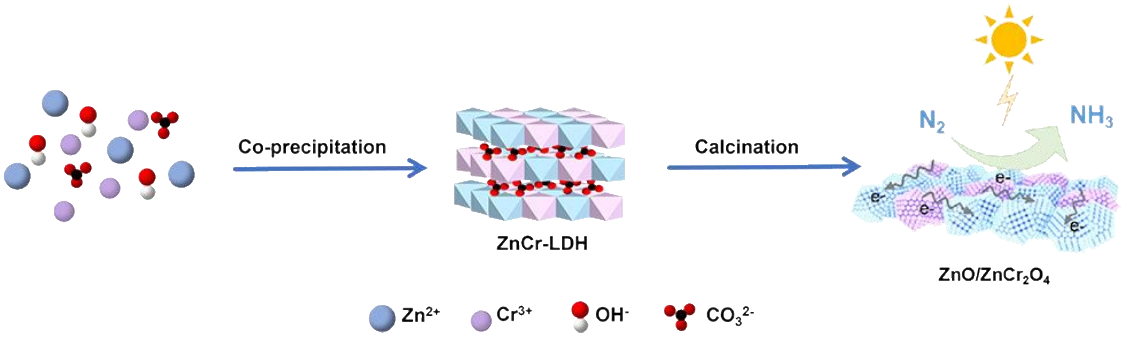

Scheme 1. Schematic illustration of the synthesis of $ZnO/ZnCr_2O_4$ heterojunction photocatalysts derived from ZnCr-LDH precursors.

Guided by the above theoretical results, we selected ZnCr-LDH as a precursor to construct the $ZnO/ZnCr_2O_4$ heterojunction photocatalysts for nitrogen photofixation. The synthesis steps for $ZnO/ZnCr_2O_4$ were depicted in Scheme 1. Firstly, the as-prepared ZnCr-LDH precursor was obtained *via* the co-precipitation method, then a series of $ZnO/ZnCr_2O_4$ heterojunction were obtained by pyrolyzing ZnCr-LDH precursor at different temperatures in the range of 300-600 °C under the oxidizing atmosphere (denoted here as Zn_XCr_1-Y, where X is the molar ratio of Zn/Cr and Y is the calcination temperature). The crystal structures of as-prepared ZnCr-LDH precursors were confirmed by powder X-ray diffraction (XRD), with all typical peaks in the XRD patterns of LDHs matching the rhombohedral LDH structure (Figure S2). In Figure 2a, new XRD reflections indexed to the hexagonal structure of ZnO (JCPDS No. 36-1451) and the cubic structure of $ZnCr_2O_4$ (JCPDS No. 22-1107) can be observed in $ZnO/ZnCr_2O_4$ derived from the Zn_XCr_1-LDH precursors at 500 °C for 2 h (named as Zn_XCr_1-5). Meanwhile, no other impurity phases can be found in Zn_XCr_1-5 samples, suggesting the successful synthesis of $ZnO/ZnCr_2O_4$. To further determine the X value in Zn_XCr_1-5, quantitative energy-dispersive X-ray spectrometry (EDS) was conducted (Figure S3-4 and Table S1-2). As shown in Figure S4 and Figure 2b, the proportion of ZnO in $ZnO/ZnCr_2O_4$ tended to rise with the Zn/Cr atomic ratio increased. In addition, the UV-vis diffuse reflectance spectroscopy of the Zn_XCr_1-5 samples (Figure S5) manifested that all Zn_XCr_1-5 samples exhibited obvious absorption ranging from 200 to 800 nm.[24-26] Moreover, high-resolution transmission electron microscopy (HRTEM)

was also utilized to characterize the structural morphologies and heterostructured interfaces of Zn_XCr_1-5 samples (Figure 2c-f). The existence of $ZnCr_2O_4$ and ZnO can be clearly observed in all Zn_XCr_1-5 samples, where the (111) and (220) planes can be identified to cubic-like $ZnCr_2O_4$. Lattice fringes with a spacing of 0.24, 0.26 and 0.28 nm are indexed to the (101), (002) and (100) crystal planes of ZnO. Obviously, the Zn_XCr_1-5 sample possessed abundant interface structures, which would enhance the photogenerated carriers' separation efficiency to promote nitrogen photofixation.

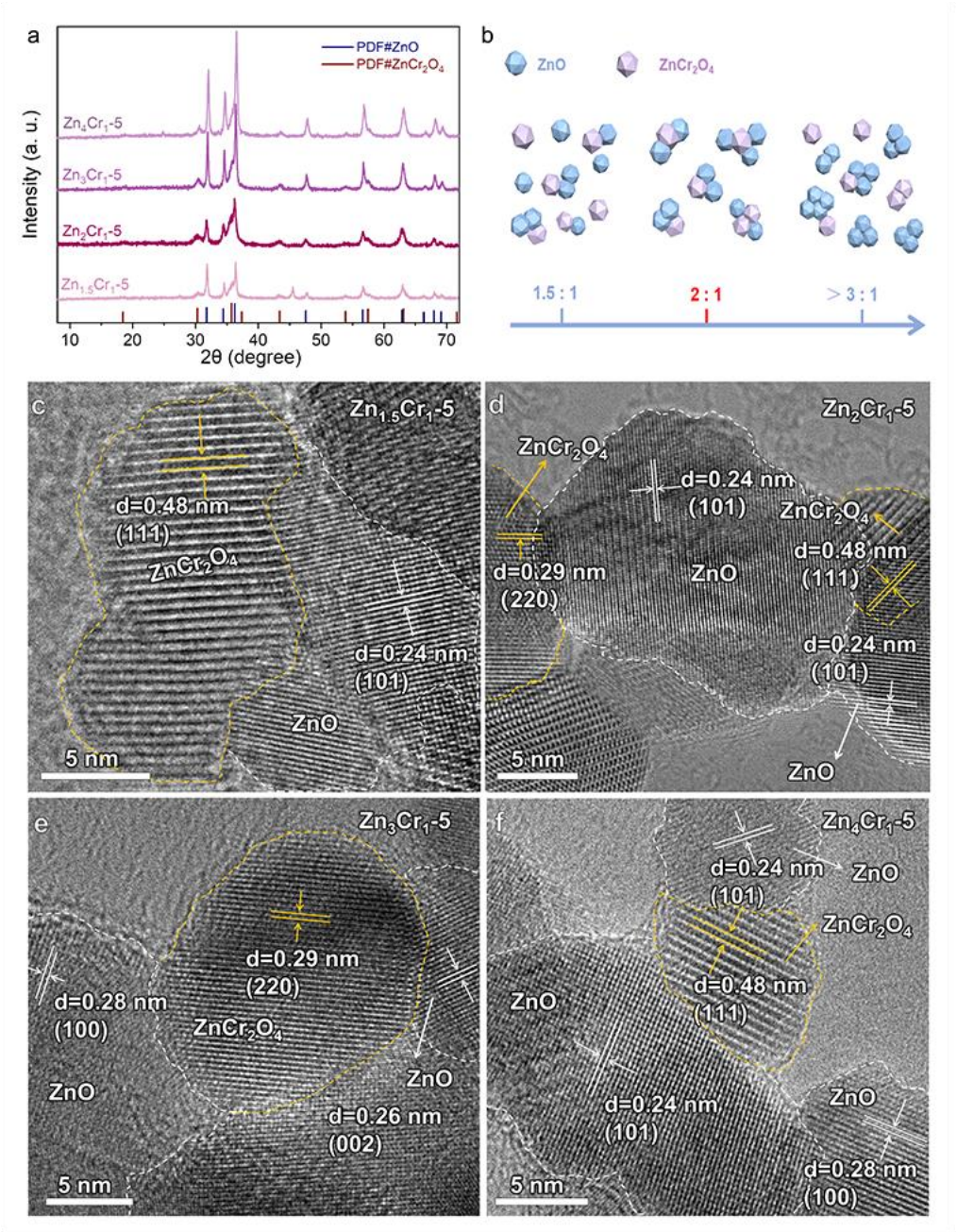

Figure 2. a) XRD patterns for Zn_XCr_1-5 photocatalysts (X = 1.5, 2, 3, and 4). b) The

schematic diagram of composition percentages for Zn_XCr_1-5 photocatalysts (X = 1.5, 2 and >3). c-f) HRTEM images for Zn_XCr_1-5 photocatalysts.

With the aim of screening the optimal composition ratio of X in Zn_XCr_1-5 samples, we subsequently evaluated their photocatalytic performance for N_2-to-NH_3 conversion in pure N_2-saturated water at ambient temperature and pressure. The product ammonia was accurately quantified *via* ion chromatography (Figure S6). As shown in Figure 3a, the NH_3 generated rate of Zn_2Cr_1-5 can reach 31.5 μmol g^{-1} h^{-1}, which is significantly higher than other Zn_XCr_1-5 samples (16.7 μmol g^{-1} h^{-1} for $Zn_{1.5}Cr_1$-5, 11.6 μmol g^{-1} h^{-1} for Zn_3Cr_1-5 and 7.5 μmol g^{-1} h^{-1} for Zn_4Cr_1-5, respectively). The better photocatalytic activity may result from the optimized heterojuncted interfaces in Zn_2Cr_1-5, leading to more efficient separation and migration of photogenerated carriers, as further demonstrated by electrochemical impedance spectroscopy (Figure S7). Additionally, to optimize ZnO/$ZnCr_2O_4$ heterojuncted interfaces derived from Zn_2Cr_1-LDH, we regulated the calcination temperature ranging from 300 to 600 °C. As shown in Figure S8, no typical XRD diffraction peaks of LDH can be observed when the Zn_2Cr_1-LDH calcined at 300 °C, illustrating the collapse of host layers in Zn_2Cr_1-LDH.[27] With the calcined temperature increased, the diffraction peaks corresponding to ZnO and $ZnCr_2O_4$ in Zn_2Cr_1-Y (Y = 4, 5, and 6) occurred, accompanied by an elevation in crystallinity. Transmission electron microscopies were carried out to directly study the morphology transformation at different temperatures (Figure S9). It can be noted that the Zn_2Cr_1-LDH exhibited a plate-like structure with a modest collapse at 300 °C, and nanoparticles (ZnO and $ZnCr_2O_4$) formed and grew when increasing the calcination temperatures to 600 °C, which is consistent with the XRD results. Based on the analyses of EDS (Figure S10 and Table S3-4), no noteworthy distinction can be identified between Zn_2Cr_1-Y samples (Y = 4, 5, and 6), indicating that the different calculation temperatures (> 400 °C) nearly have little impact on the proportion of ZnO and $ZnCr_2O_4$ in Zn_2Cr_1-Y. Moreover, the corresponding performances of Zn_2Cr_1-Y (Y = 3, 4, 5 and 6) for nitrogen photofixation were studied and displayed in Figure S11, following the order: Zn_2Cr_1-5 (31.5 μmol g^{-1} h^{-1}) > Zn_2Cr_1-6 (14.5 μmol g^{-1} h^{-1}) > Zn_2Cr_1-4 (14.3 μmol g^{-1} h^{-1}) > Zn_2Cr_1-3 (13.7 μmol g^{-1} h^{-1}). The photocatalytic performance for

amorphous Zn_2Cr_1-3 may be attributed to the abundant bulk defects.[28] With calcination temperature raised, the increased crystallinity is accompanied by a reduction in bulk defects, resulting in a better photocatalytic performance of Zn_2Cr_1-5 than that of Zn_2Cr_1-4. Additionally, particle agglomeration at 600 °C may be unfavorable to the exposure of active sites in Zn_2Cr_1-6, thereby inhibiting the improvement of photocatalytic performance. These two factors jointly influenced the separation efficiency of photogenerated carriers and exposure of the active sites, resulting in an analogous volcanic relation between calcination temperatures and ammonia production.

To further elucidate the underlying possible mechanism for the enhanced performance of heterostructured interfaces, the pristine ZnO and $ZnCr_2O_4$ samples were prepared and systematically characterized (Figure S12-13). The photocatalytic performance of as-prepared samples were evaluated under the same reaction condition as mentioned above. As observed in Figure 3b, Zn_2Cr_1-5 exhibited a superior photocatalytic activity for photocatalytic nitrogen fixation, and the NH_3 evolution rate is nearly 12 and 78 times higher than that of ZnO and $ZnCr_2O_4$ (2.5 and 0.4 μmol g^{-1} h^{-1}, respectively). In order to eliminate the effect of specific surface areas on photocatalytic performance, the Brunauer-Emmett-Teller specific surface area of each sample was further conducted (Figure S14). The normalized NH_3 production rates based on surface area (μmol m^{-2} h^{-1}) and catalyst weight (μmol g^{-1} h^{-1}) were also determined (Figure 15). A similar trend can be found that the Zn_2Cr_1-5 sample presented an outstanding ammonia evolution rate (0.82 μmol m^{-2} h^{-1}) relative to the normalized results for pure ZnO and $ZnCr_2O_4$ (0.29 and 0.005 μmol m^{-2} h^{-1}), which mainly attributes to the abundant heterostructured interfaces to dramatically improve the separation efficiency of photogenerated carriers. To further emphasize the superiority of topological transformation structure derived from LDH precursor, other ordinary ZnO/$ZnCr_2O_4$ heterojunction (denoted as ZnO/$ZnCr_2O_4$, which $ZnCr_2O_4$ grew on the seed grain of ZnO) and the physical mixture of ZnO and $ZnCr_2O_4$ (denoted as PM) were prepared for comparison (Figure S16-17). The measured results demonstrated that Zn_2Cr_1-5 photocatalyst exhibited nearly 1.9 and 3.5 times higher than that of ZnO/$ZnCr_2O_4$ and PM samples (16.6 and 9.0 μmol g^{-1} h^{-1}, respectively) (Figure 3b),

further indicating the superiority of heterojunction derived from the topological transformation of ZnCr-LDH precursor. To explore the essential difference between Zn_2Cr_1-5 and $ZnO/ZnCr_2O_4$, the fine structures of the local coordination of metal cations were analyzed using X-ray absorption fine structure (XAFS) spectroscopy. In Figure S18a-c, we can observe the XAFS data of Cr for Zn_2Cr_1-5 and $ZnO/ZnCr_2O_4$ with few distinctions, suggesting the alike local coordination of Cr cations in the two samples. Meanwhile, Zn K-edge X-ray absorption near-edge structure and corresponding extended X-ray absorption fine structure spectra for $ZnO/ZnCr_2O_4$ (Figure S18d-e) were similar to that measured in Zn_2Cr_1-5. In Figure S18f, the characteristic peaks at ~1.5 Å and ~2.8 Å in the R-space spectra could correspond to the Zn-O shell and Zn-metal shell, respectively. Notably, a longer average distance and stronger intensity of the Zn-metal shell in Zn_2Cr_1-5 in comparison to $ZnO/ZnCr_2O_4$ may be attributed to the contribution of the Zn-Zn bond originated from more adequate interfacial interactions in Zn_2Cr_1-5. Accordingly, the abundance of heterostructured interfaces would benefit the separation efficiency of photogenerated electron-hole pairs, leading to its enhanced performance for nitrogen photofixation.

In order to confirm that the NH_3 evolved from the photocatalytic N_2 reduction, various control experiments and ^{15}N isotope labeling experiments were carried out. As shown in Figure 3c, almost no ammonia was produced under all control experimental conditions. Meanwhile, the isotope labeling experiments manifested that the product of $^{15}NH_4^+$ can be detected by the indophenol blue method coupled with high-resolution mass spectroscopy when using the $^{15}N_2$ as the feed gas (Figure 3d).[29] The corresponding mass spectrometry signals at m/z = 199 and m/z = 198 are indexed to indophenol products containing ^{15}N and ^{14}N. The mass spectrometry signal at m/z = 199 was significantly enhanced when replacing the $^{14}N_2$ to $^{15}N_2$ atmosphere, further confirming that the nitrogen in NH_3 indeed originated from molecular N_2, rather than other N-containing sources. In addition, the considerable stability of Zn_2Cr_1-5 was investigated over four testing cycles, with no significant variation in photocatalytic activity and catalyst (*e.g.*, morphology, phase structure, chemical composition and valence state) observed in nitrogen photofixation (Figure S19-23). Meanwhile, the as-

prepared Zn_2Cr_1-5 sample also exhibited high photocatalytic selectivity without any NO_3^- and N_2H_4 generated during the photocatalytic test (Figure S24-25).

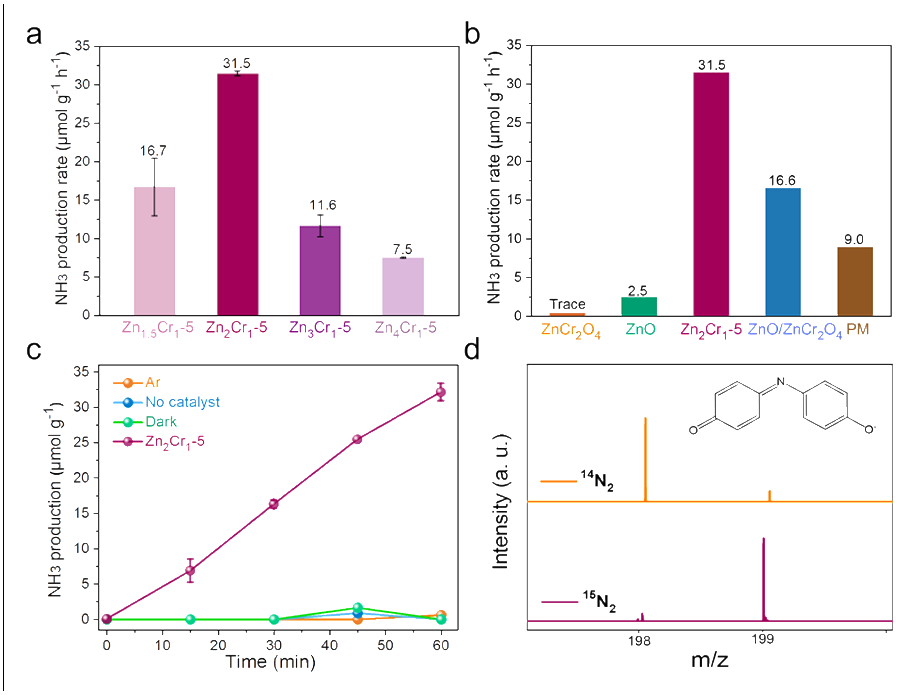

Figure 3. a-b) Photocatalytic ammonia production rates for Zn_XCr_1-5 and various contrast photocatalysts in N_2-saturated water under UV-vis irradiation. c) Time course study of photocatalytic N_2 reduction and various control experiments over Zn_2Cr_1-5. d) Mass spectra of the indophenol products obtained by reaction of phenol with ammonia generated from photocatalytic $^{14}N_2$ or $^{15}N_2$ reduction, as the chemical structure of the indophenol product responsible for the signals at m/z = 198 (containing ^{14}N) and 199 (containing ^{15}N) shown in the inset.

Since the nitrogen photoreduction process requires the transfer of multi-electron ($N_2 + 6H^+ + 6e^- \rightarrow 2NH_3$), the efficient separation efficiency of photogenerated carriers is crucial for achieving superior nitrogen photofixation performance over heterojunction photocatalysts. Therefore, the separation efficiency in Zn_2Cr_1-5 and other samples were investigated by the photoelectrochemical measurements and TS-SPV. The Nyquist plot of Zn_2Cr_1-5 in Figure 4a revealed a smaller diameter compared to other samples, indicating the lower charge-transfer resistance and more efficient electron separation in Zn_2Cr_1-5.[30] The concluded results were further confirmed by the higher intensity of photocurrent for the Zn_2Cr_1-5 sample (Figure 4b). Moreover, TS-SPV was utilized to

further understand the separation and transport of photogenerated carriers in Zn_2Cr_1-5 (Figure 4c). The photovoltage intensity generated by the sample under light is output through the conversion of the photoelectric signal. As shown in Figure 4d, the Zn_2Cr_1-5 sample possessed an enhanced photovoltage intensity compared to other samples, suggesting more efficient photogenerated carriers separation.[31] Based on these experimental results above, the optimized heterostructure interfaces in Zn_2Cr_1-5 are conducive to the separation of photogenerated carriers compared with $ZnO/ZnCr_2O_4$, which would be responsible for the enhanced performance for nitrogen photoreduction.

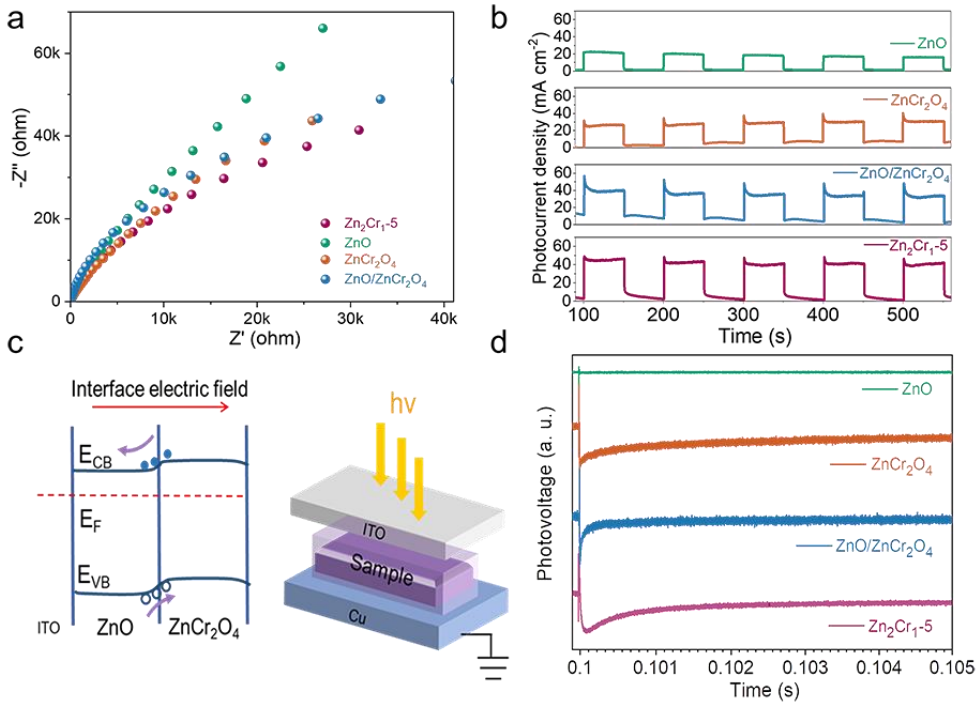

Figure 4. a-b) Electrochemical impedance spectra and the periodic on/off photocurrent response of Zn_2Cr_1-5 and other samples. c) Schematic illustrating the mechanism of transient surface photovoltage spectroscopy (ITO and Cu severally represent indium tin oxides and copper piece). d) Transient surface photovoltage spectra of Zn_2Cr_1-5 and other samples.

Conclusion

In summary, a series of $ZnO/ZnCr_2O_4$ heterojunction photocatalysts derived from ZnCr-LDH precursors were successfully synthesized by simple co-precipitation and calcination routes. By precisely tuning the heterostructured interfaces, the optimal nitrogen photofixation performance can be achieved with an NH_3 production rate of

31.5 μmol g^{-1} h^{-1} under UV-vis illumination. The excellent nitrogen photofixation performance would be ascribed to the effective separation efficiency of the photogenerated electron-hole pairs, which is facilitated by the presence of the heterostructured interfaces in $ZnO/ZnCr_2O_4$. This work provides a novel and promising approach for achieving N_2 photofixation to NH_3 over heterojunction photocatalysts derived from LDH precursors.

Supporting Information

Supporting Information is available from the Wiley Online Library or from the author.

Acknowledgments

The authors are grateful for financial support from the National Key Projects for Fundamental Research and Development of China (2018YFB1502002), the National Natural Science Foundation of China (51825205, 52120105002, 22102202, 22088102, 52072382), the Beijing Natural Science Foundation (2191002), the DNL Cooperation Fund, CAS (DNL202016), the CAS Project for Young Scientists in Basic Research (YSBR-004), and Hebei Key Laboratory of Photoelectric Control on Surface and Interface. We thank Beijing Synchrotron Radiation Facility (BSRF) for providing the EXAFS tests in 1W1B station.

Received: ((will be filled in by the editorial staff))

Revised: ((will be filled in by the editorial staff))

Published online: ((will be filled in by the editorial staff))

Conflict of interest

The authors declare no conflict of interest.

Keywords: heterojunction; layered double hydroxide; interface; photocatalysis; nitrogen fixation.

References

[1] D. E. Canfield, A. N. Glazer, P. G. Falkowski, *Science* **2010**, *330*, 192-196.

[2] J. W. Erisman, M. A. Sutton, J. Galloway, Z. Klimont, W. Winiwarter, *Nat. Geosci*. **2008**, *1*, 636-639.

[3] R. Raja, G. Sankar, J. M. Thomas, *J. Am. Chem. Soc*. **2001**, *123*, 8153-8154.

[4] V. Rosca, M. Duca, M. T. Groot, M. T. Koper, *Chem. Rev*. **2009**, *109*, 2209-2244.

[5] P. Mehta, P. Barboun, F. A. Herrera, J. Kim, P. Rumbach, D. B. Go, J. C. Hicks, W. F. Schneider, *Nat. Catal*. **2018**, *1*, 269-275.

[6] a) C. J. Van der Ham, M. T. Koper, D. G. Hetterscheid, *Chem. Soc. Rev*. **2014**, *43*, 5183-5191; b) B. K. Burgess, D. J. Lowe, *Chem. Rev*. **1996**, *96*, 2983-3012.

[7] D. Bao, Q. Zhang, F.-L. Meng, H.-X. Zhong, M.-M. Shi, Y. Zhang, J.-M. Yan, Q. Jiang, X.-B. Zhang, *Adv. Mater.* **2017**, *29*, 1604799.

[8] S. Wang, F. Ichihara, H. Pang, H. Chen, J. Ye, *Adv. Funct. Mater*. **2018**, *28*, 1803309.

[9] a) A. J. Medford, M. C. Hatzell, *ACS Catal*. **2017**, *7*, 2624-2643; b) R. Schlögl, *Angew. Chem. Int. Ed*. **2003**, *42*, 2004-2008.

[10] A. Banerjee, B. D. Yuhas, E. A. Margulies, Y. Zhang, Y. Shim, M. R. Wasielewski, M. G. Kanatzidis, *J. Am. Chem. Soc.* **2015**, *137*, 2030-2034.

[11] S. Lin, X. Zhang, L. Chen, Q. Zhang, L. Ma, J. Liu, *Green Chem.* **2022**, *24*, 9003-9026.

[12] a) H. Li, J. Shang, J. Shi, K. Zhao, L. Zhang, *Nanoscale* **2016**, *8*, 1986-1993; b) A. Kudo, Y. Miseki, *Chem. Soc. Rev.* **2009**, *38*, 253-278.

[13] a) A. Furube, T. Asahi, H. Masuhara, H. Yamashita, M. Anpo, *J. Phys. Chem. B* **1999**, *103*, 3120-3127; b) M. R. Gholipour, C. T. Dinh, F. Béland, T. O. Do, *Nanoscale* **2015**, *7*, 8187-8208.

[14] a) H. Hirakawa, M. Hashimoto, Y. Shiraishi, T. Hirai, *J. Am. Chem. Soc*. **2017**, *139*, 10929-10936; b) J. Di, J. Xia, M. F. Chisholm, J. Zhong, C. Chen, X. Cao, F. Dong, Z. Chi, H. Chen, Y. Weng, J. Xiong, S. Yang, H. Li, Z. Liu, S. Dai, *Adv. Mater.* **2019**, *31*, 1807576.

[15] Y. Wei, W. Jiang, Y. Liu, X. Bai, D. Hao, J.-B. Ni, *Nanoscale* **2022**, 14, 2990-2997.

[16] S. Liu, M. Wang, H. Ji, L. Zhang, J. Ni, N. Li, T. Qian, C. Yan, J. Lu, *Adv. Mater.* 2023, 35, 2211730.

[17] G. Cui, W. Wang, M. Ma, J. Xie, X. Shi, N. Deng, J. Xin, B. Tang, *Nano Lett*. **2015**, *15*, 7199-7203.

[18] a) X. Zhang, Y. Zhao, Y. Zhao, R. Shi, G. I. N. Waterhouse, T. Zhang, *Adv. Energy Mater.* **2019**, *9*, 1900881; b) S. Zhang, Y. Zhao, R. Shi, C. Zhou, G. I. N. Waterhouse, L.-Z. Wu, C.-H. Tung, T. Zhang, *Adv. Energy Mater.* **2020**, *10*, 1901973; c) S. Nayak, L. Mohapatra, K. Parida, *J. Mater. Chem. A* **2015**, *3*, 18622-18635; d) L. Mohapatra, K. Parida, *J. Mater. Chem. A* **2016**, *4*, 10744-10766.

[19] a) M.-Q. Zhao, Q. Zhang, W. Zhang, J.-Q. Huang, Y. Zhang, D. Su, F. Wei, *J. Am. Chem. Soc.* **2010**, *132*, 14739-14741; b) X. Jia, Y. Zhao, G. Chen, L. Shang, R. Shi, X. Kang, G. I. N. Waterhouse, L.-Z. Wu, C.-H. Tung, T. Zhang, *Adv. Energy Mater.* **2016**, *6*, 1502585.

[20] F. H. Abdullah, N. A. Bakar, M. A. Bakar, *J. Hazard. Mater.* **2021**, *406,* 124779.

[21] T. Dixit, A. Kumar, I. A. Palani, V. Singh, *Scr. Mater*. **2016**, *114*, 84-87.

[22] Z. Mousavi, F. Soofivand, M. Esmaeili-Zare, M. Salavati-Niasari, S. Bagheri, *Sci. Rep*. **2016**, *6*, 1-18.
[23] a) G. Thennarasu, A. Sivasamy, *J. Chem. Technol. Biot*. **2015**, *90*, 514-524; b) P. Parhi, V. Manivannan, *J. Eur. Ceram. Soc*. **2008**, *28*, 1665-1670.
[24] S. Zhang, Y. Zhao, R. Shi, C. Zhou, G. I. N. Waterhouse, Z. Wang, Y. X. Weng, T. Zhang, *Angew. Chem. Int. Ed.* **2021**, *60*, 2554-2560.
[25] T. Dixit, J. Agrawal, *IEEE Electron Device Lett.* **2019**, *40*, 1143-1146.
[26] X. Han, B. Liu, J. Sun, *Acta Phys.-Chim. Sin*. **1994**, *10*, 978-985.
[27] Z. Li, J. Liu, Y. Zhao, R. Shi, G. I. N. Waterhouse, Y. Wang, L.-Z. Wu, C.-H. Tung, T. Zhang, *Nano Energy* **2019**, *60*, 467-475.
[28] Y. Xu, Z. Wang, L. Tan, Y. Zhao, H. Duan, Y.-F. Song, *Ind. Eng. Chem. Res.* **2018**, *57*, 10411-10420.
[29] Y. Zhao, R. Shi, X. Bian, C. Zhou, Y. Zhao, S. Zhang, F. Wu, G. I. N. Waterhouse, L.-Z. Wu, C.-H. Tung, T. Zhang, *Adv. Sci*. **2019**, *6*, 1802109.
[30] L. Lv, Y. Chang, X. Ao, Z. Li, J.-G. Li, Y. Wu, X. Xue, Y. Cao, G. Hong, C. Wang, *Mater. Today Energy* **2020**, *17*, 100462.
[31] M. Li, S. Yu, H. Huang, X. Li, Y. Feng, C. Wang, Y. Wang, T. Ma, L. Guo, Y. Zhang, *Angew. Chem. Int. Ed.* **2019**, *58*, 9517-9521.

Advanced $ZnO/ZnCr_2O_4$ photocatalysts derived from ZnCr-layered double hydroxide (ZnCr-LDH) precursors are successfully synthetized by a simple thermal process. The optimized $ZnO/ZnCr_2O_4$ exhibit a considerable ammonia photosynthesis rate of 31.7 $\mu mol\ g^{-1}\ h^{-1}$ in pure water, with the origin of the high activity being derived from the high-efficiency carrier separation due to the abundant interfaces.

Keywords: heterojunction; layered double hydroxide; interface; photocatalysis; nitrogen fixation.

Junyu Gao, Fan Wu, Yunxuan Zhao, Xuanang Bian, Chao Zhou, Junwang Tang and Tierui Zhang**

Tuning the Interfaces of $ZnO/ZnCr_2O_4$ Derived from Layered-Double-Hydroxide Precursors to Advance Nitrogen Photofixation

ToC figure: